湖南大学学报（自然科学版）
Journal of Hunan University (Natural Sciences)

第 50 卷 第 9 期
2023 年 9 月

Available online at http://jonuns.com/index.php/journal/index

Vol. 50 No. 9
September 2023

Open Access Article

https://doi.org/10.55463/issn.1674-2974.50.9.8

Experimental Investigation of Self-Cleaning Behavior of 3D-Printed Textile Materials with Different Printing Parameters

Ibrahim Sabry[1], Abdel-Hamid Ismail Mourad[2,3,4], Heba Atef Abd El-Aziz[5], A.M Hewidy[1]

[1] Department of Mechanical Engineering, Faculty of Engineering, Benha University, Benha, 13511, Egypt

[2] Mechanical and Aerospace Engineering Department, College of Engineering, United Arab Emirates University, Al-Ain, 15551, United Arab Emirates

[3] National Water and Energy Center, United Arab Emirates University, Al Ain, 15551, United Arab Emirates

[4] On leave from the Mechanical Design Department, Faculty of Engineering, Helwan University, El Mataria, Cairo, Egypt

[5] Printing, Dyeing and Finishing Department, Faculty of Applied Arts, Benha University, Benha, Egypt

Received: June 8, 2023 / Revised: July 4, 2023 / Accepted: August 12, 2023 / Published: September 29, 2023

Abstract: The ability to eliminate contaminants from the surface without an external source is a characteristic feature of self-cleaning textile fabrics. This advanced application of science is environmentally friendly because it saves on laundry, water, electricity, and other resources and money. In the past, the self-cleaning feature was typically acquired through chemical coatings, which enhance the roughness and lower the surface energy of the fabric, thereby causing the particle or droplet pollutants to float over the surface layer instead of adhering to it. This technique works well for fabrics manufactured using conventional woven-based textile technology. The production of textile fabrics has changed recently, thanks to paid advances in technologies such as 3D printing. However, the earlier chemical coating-based technique cannot clean printed fabrics in such a way. A developed regression model to study the relationship between the secondary 3D printing parameters and the self-cleaning capabilities of various polymeric textiles allowed a deeper investigation. This study aims to examine the effects of the primary printing factors, such as the flow rate, printing temperature, and speed printing, on the self-cleaning characteristics of the printed textile. We measured the self-cleaning behavior of the chosen material, polyurethane fabric, used the trial findings to build a regression polynomial, and empirically validated models to show the critical values of the main parameters considered for the ideal self-cleaning behavior. The outcome indicated the processing-property relationship of the parts, including determining the most vital parameters that influence the fabric's wettability.

Keywords: self-cleaning, 3D printing, polyurethane, design of experiments, optimization.

不同列印參數三維印刷紡織材料自清潔行為的實驗研究

摘要：無需外部來源即可消除表面污染物的能力是自清潔紡織布料的一個特徵。這種先進的科學應用是環保的，因為它可以節省洗衣、水、電力以及其他資源和金錢。過去，自清潔功能通常是透過化學塗層獲得的，化學塗層增強了織物的粗糙度並降低了表面能，從而使顆粒或液滴污染物漂浮在表面層上，而不是黏附在表面層上。此技術適用於使用傳統機織紡織技術製造的織物。由於三維 列印等技術的進步，紡織面料的生產最近發生了變化。然而，

早期基於化學塗層的技術無法以這種方式清潔印花織物。所開發的迴歸模型用於研究二次三維 列印參數與各種聚合物紡織品的自清潔能力之間的關係，從而可以進行更深入的研究。本研究旨在探討主要印刷因素（例如流量、印刷溫度和印刷速度）對印刷紡織品自清潔特性的影響。我們測量了所選材料（聚氨酯織物）的自清潔行為，利用試驗結果建立回歸多項式，並透過經驗驗證模型來顯示理想自清潔行為所考慮的主要參數的臨界值。結果顯示了部件的加工性能關係，包括確定影響織物潤濕性的最重要參數。

关键词：自清潔、三維列印、聚氨酯、實驗設計、最佳化。

1. Introduction

Developing the self-cleaning feature in textile products eliminates contaminants from the textile fabric without the assistance of an outside source [1], thereby substantially reducing the amount of water and energy required in the laundry. The surface of such fabrics is typically designed to be hydrophobic in nature [2] and takes its cue from the behavior of the lotus leaf, in which liquid droplets falling onto its surface pick up dirt particles and cause them to roll or glide down the leaf surface [3]. Several forces influence the hydrophobic self-cleaning qualities discussed, including those acting on the particle at the water–air interface, the textile surface, and the gravitational and buoyant forces of the pollutant particles.

The wettability factor also influences it, which measures the particle's contact angle with the surface [2]. The discussed forces influence microscale characteristics, including friction, adhesion, surface roughness, and surface-free energy [3]. It is difficult to conceive and quantify the interdependencies between the characteristics and the forces affecting them [2]. Recent developments in 3D printing technology have demonstrated their promise for use in the textile sector [5, 58, 60], particularly in self-cleaning [4].

3D printing on textile substrates [6] and 3D printing of whole textile products are various forms of 3D printing applications for textiles [7, 59]. Partsch et al. investigated the textile characteristics of a 3D-printed acrylonitrile butadiene styrene (ABS) sample for textile 3D printing [8]. To create tulle-like materials on standard fused deposition modeling (FDM) printers, [9] proposed the 'DefeXtiles technology', based on the controlled extrusion of filaments. [10] employed a regulated printer head motion to print fibers across a row of pillars, which supports fiber deposition and forms a framework. Chainmail, weft knit, and printed sheets were among the 3D-printed textile structures fabricated by the above technique. Chainmail refers to tiny, interlocking pieces that may be bent and customized, whereas the weft knit structure can be knitted using 3D printing. The printed sheet under investigation here refers to a single-layer or multi-layer mesh structure created using 3D printing in several studies [11, 57].

Several developed 3D-printed textiles had self-cleaning capabilities, including advantages such as waterproof and dustproof characteristics. For instance, a recent study investigated the possible uses of tissue-supporting devices such as ankle or knee braces made of thermoplastic polyurethane (TPU) mesh that is 3D printed [11] using TPU filament [12], demonstrating how mechanical properties can be tailored digitally using control and optimization of the toolpath during the extrusion process. Similarly, they must have surface characteristics of 3D-printed materials that can fully realize discussed self-cleaning capabilities.

From existing literature studies, it is evident that chemical coatings induce self-cleaning behavior in textile materials. However, using traditional chemical coating techniques to achieve self-cleaning behavior is challenging in 3D-printed fabrics [13]. To produce textile fabrics with self-cleaning features, textile manufacturing using 3D printing techniques must incorporate alternative methods, such as close control of the printing conditions during the fabrication stage, highlighted in several studies. The behavior of self-cleaning FDM-based structures has been analyzed [14], including methods in which a superhydrophobic surface uses a dip coating technique of silica nanoparticles [15]. Such a surface was developed by controlling the printing parameters and polymer material properties [16]. The study draws several vital relationships between the processing parameters and the final mechanical part properties, such as an increase in the infill density of polyethylene terephthalate glycol (PETG) in FDM results in an increase in the specimen's tensile strength, the surface roughness and self-cleaning behavior diminishes [17, 29, 54].

In another study, polylactic acid (PLA) printed cubic pieces showed decreasing surface roughness and a modest increase in porosity as a function of printing temperature, speed, and flow rate [18]. In comparison, the flow rate and printing acceleration hugely affected the surface roughness and wettability of a 3D-printed PETG rectangular specimen, followed by layer height

and print temperature. Additionally, a recent study used the response surface methods (RSM) to construct a mathematical model to analyze the relationship of the FDM printing parameters, including layer thickness, orientation angle, and infill angle, to the surface roughness of the ABS-printed parts [19]. For single- and multi-objective optimization and modeling construction for FDM printed PLA models, another study [20] successfully employed the Taguchi method and RSM. The optimized results recommended by the RSM models empirically confirmed the correctness of the Taguchi method and the printing parameters' robustness.

However, all the above investigations concentrated on 3D-printed structures rather than the specific case of textiles. Despite the importance of surface-level research covered by most published articles on printed structures and their self-cleaning behavior, the available literature still lacks a thorough quantitative understanding to establish the relationships between the principal printing parameters and the described behavior. The authors recently developed a linear regression model [1, 21, 56] to show the quantitative relationship between the secondary 3D printing parameters and the self-cleaning qualities of various polymeric textiles. In their earlier research, the effect of printing parameters on three different materials – thermoplastic elastomer (TPE), thermoplastic polyurethane (TPU), and thermoplastic copolyester (TPC) – was examined. The secondary printing parameters of layer height, extruder width, and angular orientation were successfully optimized using a linear regression model to provide the optimal self-cleaning surface feature measured concerning surface roughness, wettability, and porosity.

For many applications that require outdoor surfaces with significant surface area, surfaces with low affinity to water are becoming increasingly common [42]. Because of their inherent hydrophobicity, they are excellent candidates for self-cleaning [43], anti-icing [44], and anti-corrosion applications.

Because of the small surface area in contact with water, the possibility of such surfaces interacting with aqueous species to create chemical interactions is relatively low. High water contact angles – typically greater than 100° and occasionally 150°, in which case the coatings are superhydrophobic – a distinguishing feature of hydrophobic coatings [45]. Surface chemistry and surface roughness need to be regulated simultaneously to produce (hyper) hydrophobic surfaces. Using several approaches, including sol–gel [46], co-condensation [47], layer-by-layer deposition [48], chemical deposition [49], electrospinning [50], hydrothermal synthesis [51], and lithographic techniques [52], numerous artificial hydrophobic surfaces have been created based on this theory.

The study also discovered that TPE has the best overall self-cleaning behavior, followed by TPU and TPC materials [22, 30] when evaluated under the abovementioned criteria. However, TPE was erratic during printing, leading to low-grade fabrics, and TPU appeared more appropriate than the other two materials.

After analyzing the results obtained from previous studies, this paper examined the effect of the basic 3D printing settings on the self-cleaning behavior of the TPU. The key printing parameters considered in this study include flow rate, printing temperature, and printing speed. The authors built regression polynomials using the trial findings to quantify the self-cleaning behavior of the chosen fabric and experimentally evaluated models to highlight the crucial values of the primary parameters considered for the best self-cleaning.

2. Materials and Methods

2.1. Specimen Preparation

Kodak Flex 98 flexible TPU filament was used for printing the textile structures. Table 1 contains all vital process parameters and their levels of magnitude selected for the study. The geometry of the fabric was modeled in SolidWorks 2021 with dimensions of 100 mm × 80 mm × 0.4 mm to make a comparative study with earlier works [21, 35]. The fabric model was then exported as an STL file and prepared for printing using the optimal secondary printing settings from previous works related to TPU. The printing process parameter settings fixed in the study include:

- Layer height: 0.18 mm;
- Extrusion width: 0.7 mm;
- Cross-raster orientation: 75^{o};
- Bed temperature: 35^{0}C.

The 3D printer software sliced the model with printing parameters set before sending the g-code file to the Raise 3D Pro 2 printer for production.

2.2. Design of Experiments

The three printing factors examined in this study were selected after considering their substantial influence on self-cleaning behavior [41]. Table 1 shows three levels of higher, median, and lower values of each parameter determined by trial and error. There were 27 different parameter combinations because of the complexity of the printing parameter variables and levels. To examine all the experimental variables with the fewest possible tests, specialized orthogonal arrays were employed. The Design of the Experiment program, Design Expert®, was used to produce the full factorial 27 orthogonal array displayed in Table 2. It produced the 27 different parameter combinations needed for the experiment. For every combination, three samples were printed and tested to ensure reproducibility of the results. Each got a name based on the run number and from bottom to top (1 is the bottom sample, and 3 is the top sample in the printing order).

The printed specimens had an average strand distance of approximately 0.1 mm.

Table 1 Levels of process parameters in the FDM printing of TPU

Process parameters	Unit	Symbol	Level		
			1	**2**	**3**
Flow rate	%	R	50	100	150
Printing speed	mm/min	S	30	40	50
Printing temperature	C	T	230	240	250

Table 2 Full factorial results for average self-cleaning features code

Run	Printing temperature	Printing speed	Flow rate	Porosity	SR-X	SR-Y	Standard deviation
1	2.333	-3.000	-2.000	11.896	11.05	10.6232	10
2	2.333	-1.000	-2.000	10.67	18.26	18.00074	9
3	2.333	1.000	-2.000	12.244	15.52	18.26074	27
4	1.667	-3.000	-2.000	16.4126	11.7	12.342	7
5	1.667	-1.000	-2.000	11.8688	18.27	18.26074	22
6	1.667	1.000	-2.000	26.536	15.91	17.26074	25
7	1.000	-3.000	-2.000	15.8382	10.93	11.2607	13
8	1.000	-1.000	-2.000	16.8469	18.19	17.81699	2
9	1.000	1.000	-2.000	14.38	14.91	15.26074	15
10	2.333	-3.000	-1.000	33.43	11.24	11.2607	23
11	2.333	-1.000	-1.000	35.58	19.1	18.43949	4
12	2.333	1.000	-1.000	32.83	15.32	14.07699	8
13	1.667	-3.000	-1.000	12.84	18.91	18.89824	11
14	1.667	-1.000	-1.000	16.22	17.92	17.17949	6
15	1.667	1.000	-1.000	8.841	15.75	15.44449	5
16	1.000	-3.000	-1.000	71.12	11.47	11.2607	24
17	1.000	-1.000	-1.000	29.57	18.91	18.26074	18
18	1.000	1.000	-1.000	19.938	15.84	15.26074	14
19	2.333	-3.000	0.000	12.47	11.25	11.2607	16
20	2.333	-1.000	0.000	22.87	19.29	19.26074	19
21	2.333	1.000	0.000	15.53	16.42	16.26074	17
22	1.667	-3.000	0.000	214.48	11.34	11.2607	21
23	1.667	-1.000	0.000	51.36	19.56	19.26074	26
24	1.667	1.000	0.000	15.76	16.64	16.52074	12
25	1.000	-3.000	0.000	19.23	15.2	15.26074	20
26	1.000	-1.000	0.000	8.2	16.54	16.08199	1
27	1.000	1.000	0.000	3.15	17.6	17.70449	3

Fig. 1 illustrates the rationale and flow of the experiment. The response optimizer created a mathematical model based on the RSM approach and used it for optimization. To create a suitable functional relationship between the response of interest and the control variables, RSM uses statistical and mathematical approaches [23]. The printing parameters and self-cleaning characteristics were then fitted using a second-order regression model, as shown in equations (1) and (2). In this scenario, y is the response variable, b_0 is a constant, b_1, b_2, and b_k are coefficients, and x_1, x_2, and x_k are control variables and is the error term. The weighted individual desirability of each response result was determined using Minitab according to its significance. The calculated composite desirability of the multi-response system combined these values and generated the ideal solution when the level of desirability was highest. The mathematical model was further validated by printing the proposed optimized solutions and comparing them with the empirical findings.

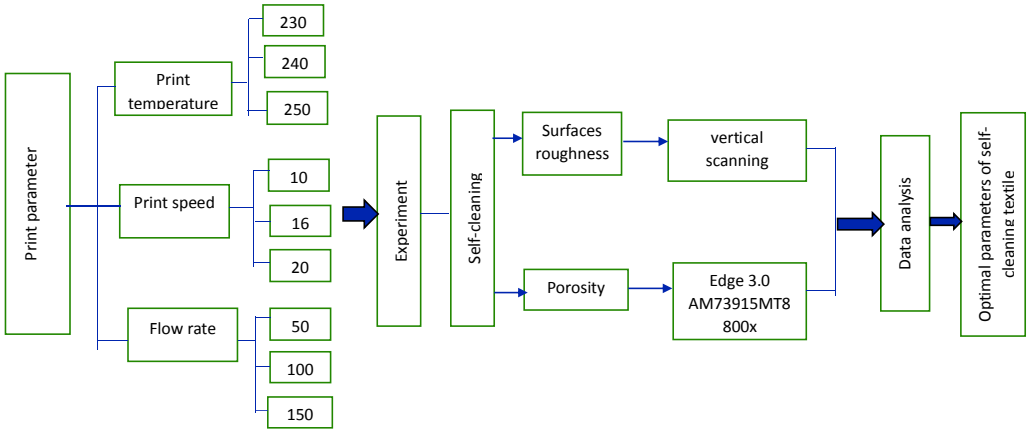

Fig. 1 Flowchart of the experiment

The flow rate (R), printing temperature (T), and speed (S) were independent process parameters

affecting porosity (P), surface roughness (SR-x), and surface roughness (SR-y) measured in two perpendicular x and y directions, respectively, based on preliminary testing and earlier investigations.

$$X_i = 2X - \frac{X_{max} + X_{min}}{X_{max} - X_{min}} \quad (1)$$

where X_i, X, X_{min}, and X_{max}, represent the needed coded value of any variable, variable value, variable's lower limit, and variable's upper limit, respectively [24].

Table 2 depicts the design matrix. The porosity, surface roughness-x, and roughness-y, which are measures of the self-cleaning characteristics, are functions of the flow rate, printing speed, and temperature. Therefore, the relationship between these variables is

$$Y = f(R, T, S) \quad (2)$$

where Y is the response, T is the rotation speed, S is the shoulder diameter, and R is the travel speed. The chosen polynomial can be written as follows in terms of the three factors:

$$\beta_0 + \beta_1 R + \beta_2 T + \beta_3 S + \beta_{11} R^2 + \beta_{22} T^2 + \beta_{33} S^2 + \beta_{12} TR + \beta_{13} RS + \beta_{23} TS \quad (3)$$

where 0 is the free term of the regression equation; 1, 2, 3 are linear coefficients; 11, 22, 33 are quadratic coefficients; 12, 13, 23 are interaction coefficients.

The regression analysis uses the following equations to determine the polynomial coefficient values:

$$\beta_0 = 0.1663 \sum(Y) - 0.0568 \sum\sum(X_{ii} Y) \quad (4)$$

$$\beta_j = 0.0732 (X_i Y) \quad (5)$$

$$\beta_j = 0.0625 \sum(X_{ii} Y) + 0.00689 \sum\sum(X_{ii} Y) - 0.0568 \sum(Y) \quad (6)$$

$$\beta_{ij} = 0.1250 \sum(X_{ij} Y) \quad (7)$$

where $i, j = 1, 2, 3$, and $I < j$

2.3. Measurement of the Surface Roughness

The Time 3220 Surface Roughness Tester recorded the surface roughness measurement in the experimental investigation illustrated in Fig. 2. The average standard deviation of the measurements defined the surface roughness, and a significant peak in the recorded surface profile indicates a greater roughness. Any water or liquid droplet impinging on the sample surface will travel along the surface shape without entering the pores if the peaks are too high.

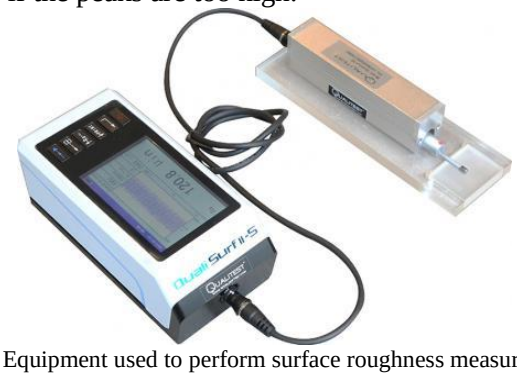

Fig. 2 Equipment used to perform surface roughness measurements

The initial step in the measurement process was to obtain the physical sample surface roughness parameters (Ra) [31, 32]. As shown in Fig. 3, the filtered profiles were used to calculate the surface roughness Ra expressed quantitatively.

2.4. Measurement of the Porosity Values

Between fibers and yarns, a textile's structure includes pores, and porosity can be defined as the void-to-volume ratio within the confines of a solid material [37]. Fig. 4 illustrates how fabric geometry affects its pore size and distribution, including the characterization results. On the basis of the various levels of selected experimental print settings, the porosity characteristics were examined and optimized [38, 39, 55].

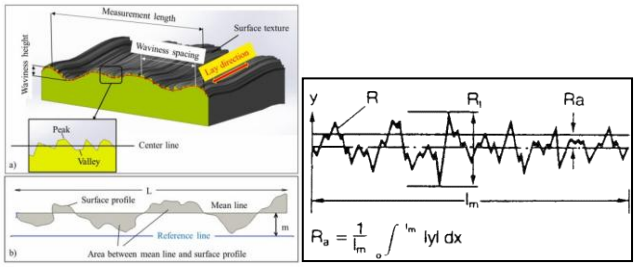

Fig. 3 Example of (a) surface texture, (b) surface roughness (Ra) terminology [27], and (c) peak height profile

The main benefits of employing digital image analysis to determine a textile sample's porosity include increased accuracy and duplicability. A Dino-lite digital microscope captured digital photographs of a portion of the specimens. The colored photos of the fabrics were later converted to grayscale, loaded into a computer, and transformed into binary images using known magnifications. The fabric's entire area and porous area were then retrieved.

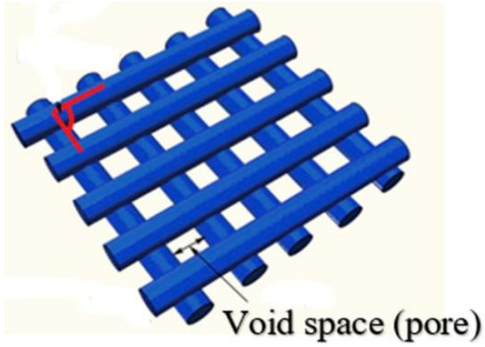

(a)

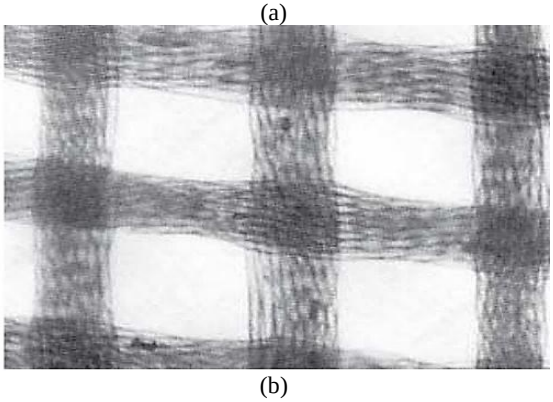

(b)

Fig. 4 Example of (a) porosity of textile fabrics and (b) porosity measurement method

3. Results and Discussion

The key finding from the research was that the flow rate was the most influential printing parameter in controlling the self-cleaning characteristics measured by characteristics such as surface roughness and porosity, followed by print temperature and speed. These results agree with the outcomes of earlier works [20, 21], thereby showcasing the effectiveness of the study. The surplus filament squeezed by the nozzle head flowed into the surrounding area, which is a straightforward explanation for why the flow rate is the essential printing parameter affecting porosity and surface roughness. The height difference between the first and second layers was reduced because they filled the space between the printed filament line [40]. The print speed affects the geometry of the filament. High print speeds resulted in a continuous filament deposit and a smaller acceleration and deceleration zone. As a result, there was a smaller gap between each filament, resulting in low porosity values that continued until the nozzle head experienced excessive acceleration and deceleration at sample runs close to 20 mm/min print speed, which caused the filament to become unstable and separate from the print bed. As a result, there was an increase in the space between filaments, which produced significant porosity.

Table 2 contains the average outcomes of the study and their standard deviation (SD) for the 27 runs, with triplicate testing performed for each sample. Even though all three input parameters were the experiment's dependent variables, this study examined their correlation because numerous other studies have already demonstrated the impact of surface roughness (SR). On the other hand, SR first increases noticeably when porosity (PT) increases and then marginally decreases following, noticeable by the related p-values of the Pearson correlation coefficient explained in the forthcoming sections. The highest value represents the ideal parameter settings for the largest SR, which here are a flow rate of 50%, printing speed of 20 mm/s, and temperature of 240^{0}C.

As it affects the size and number of holes in the textile fabric, the porosity should be as low as can be achieved practically. Fig. 5 displays the porosity main effect plot for each printing setting. The fact that there is a 12.96% difference between the highest and lowest average porosity indicates that flow velocity is the primary factor affecting porosity. Fig. 5 also shows the flow rate's main impact on each level.

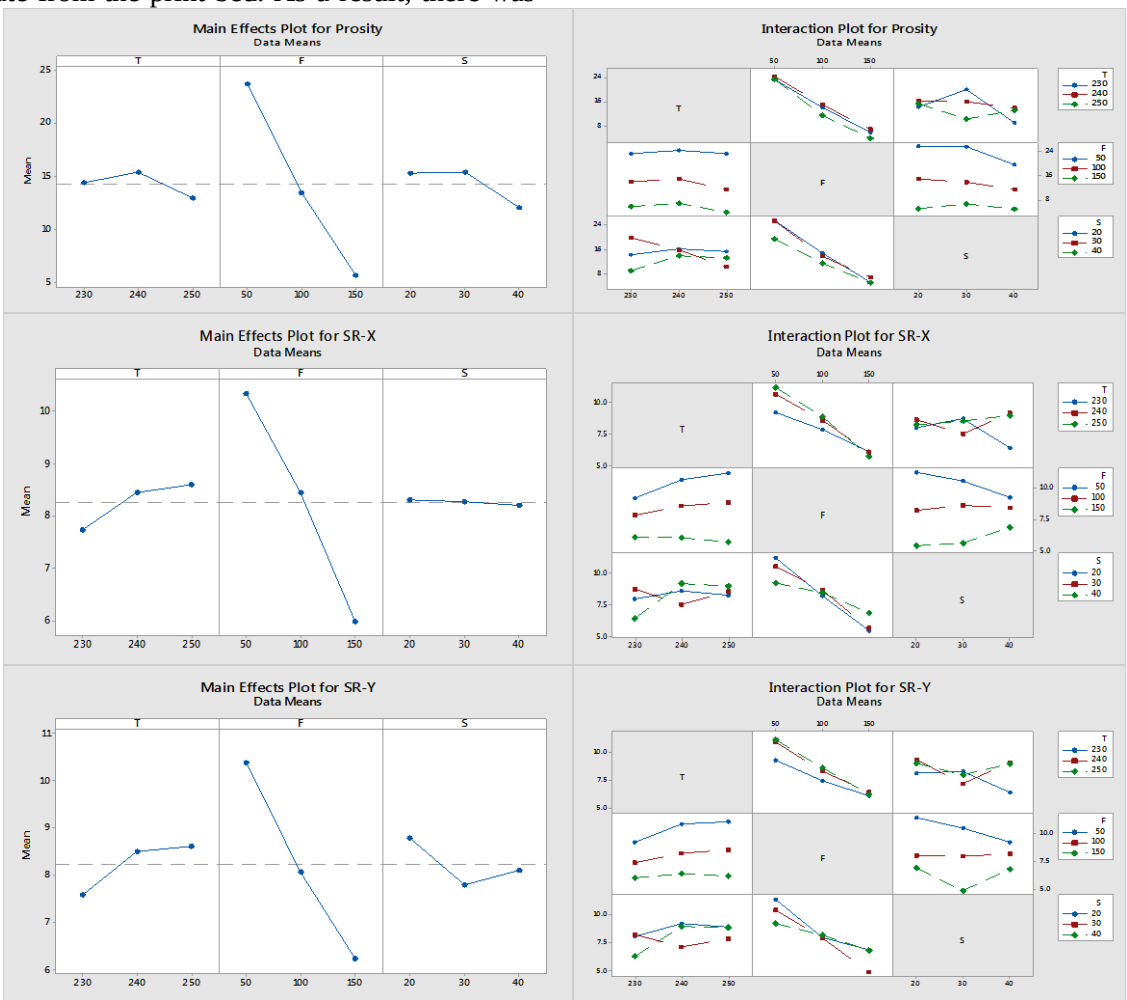

Fig. 5 (a) Main effects plot and (b) interaction plot for mean values of (i) porosity, (ii) SR-x, and (iii) SR-y

It is crucial to note that level 2 values for different printing parameters produce peaks or minima within a constrained range. To fully comprehend these trends, further study is required. For the smallest porosity and

SR, a print speed of 40 mm/s, a print temperature of 230^0C, and a flow rate of 50% are the optimal parameter settings.

The ANOVA method validates that the final developed regression connections are appropriate. The constructed model's acceptability (for example, 95%) corresponds to the estimated F-ratio value less than the standard F-ratio value from the F-table at the stated degree of confidence [25]. Table 3 lists the porosity ANOVA results, whereas Table 4 and Table 5 display the SR ANOVA results according to the direction of investigation. According to the statistical study that considered the three major process parameters and three levels of process magnitude, it was clear that none of the main effects of the parameters or their interactions had any bearing on the porosity because their p values were more than 0.05 with a 95% confidence interval. From the surface roughness study results, the interaction between the flow rate and printing temperature was significant (p-value<0.05), as seen from the interaction plot in Fig. 5. However, the interaction between the flow rate and printing speed was not significant enough (p-value>0.05).

Table 3 Porosity ANOVA results

Source	Sum of squares	df	Mean Square	F-value	p-value	
Model	1593.34	9	177.04	11.61	< 0.0001	Significant
A-Temp.	1.64	1	1.64	0.1077	0.7468	
B-Flow Rate	54.82	1	54.82	3.59	0.0751	
C-Speed	4.04	1	4.04	0.2650	0.6133	
AB	17.03	1	17.03	1.12	0.3055	
AC	10.21	1	10.21	0.6695	0.4246	
BC	28.16	1	28.16	1.85	0.1919	
A^2	3.23	1	3.23	0.2118	0.6512	
B^2	8.92	1	8.92	0.5850	0.4548	
C^2	2.79	1	2.79	0.1831	0.6741	
Residual	259.26	17	15.25			
Lack of fit	106.77	5	21.35	1.68	0.2136	Not significant
Pure Error	152.49	12	12.71			
Cor Total	1852.60	26				

Table 4 SR-x ANOVA results

Source	Sum of squares	df	Mean square	F-value	p-value	
Model	114.51	9	12.72	11.96	< 0.0001	Significant
A-Temp.	0.5360	1	0.5360	0.5037	0.4875	
B-Flow Rate	10.38	1	10.38	9.76	0.0062	
C-Speed	0.0491	1	0.0491	0.0462	0.8324	
AB	7.55	1	7.55	7.09	0.0164	
AC	0.0681	1	0.0681	0.0640	0.8033	
BC	13.42	1	13.42	12.61	0.0025	
A^2	0.2791	1	0.2791	0.2623	0.6152	
B^2	0.4779	1	0.4779	0.4491	0.5118	
C^2	0.0954	1	0.0954	0.0897	0.7682	
Residual	18.09	17	1.06			
Lack of Fit	5.36	5	1.07	1.01	0.4534	Not significant
Pure Error	12.73	12	1.06			
Cor Total	132.60	26				

Table 5 SR-y ANOVA results

Source	Sum of squares	df	Mean square	F-value	p-value	
Model	112.07	9	12.45	8.63	< 0.0001	Significant
A-Temp.	1.01	1	1.01	0.6974	0.4153	
B-Flow Rate	12.76	1	12.76	8.84	0.0085	
C-Speed	0.2310	1	0.2310	0.1602	0.6940	
AB	12.49	1	12.49	8.66	0.0091	
AC	0.5046	1	0.5046	0.3499	0.5620	
BC	6.75	1	6.75	4.68	0.0450	
A^2	0.7229	1	0.7229	0.5012	0.4886	
B^2	0.3512	1	0.3512	0.2435	0.6280	
C^2	1.55	1	1.55	1.07	0.3145	
Residual	24.52	17	1.44			
Lack of Fit	8.05	5	1.61	1.17	0.3776	Not significant
Pure Error	16.47	12	1.37			
Cor Total	136.59	26				

3.1. Process Parameter Optimization

Fig. 5 depicts the impact of self-cleaning for 3D-printed textile parameter settings on porosity in the perturbation plot in the case of an optimum design. The optimization of printing parameters was modeled to achieve the best self-cleaning ability of the printed

specimens. The devised method and optimization model can be used to estimate the self-cleaning of the printed fabric if the inputs of the printing parameters are known. We can attain even better self-cleaning behaviors if we provide various combinations of these parameters and establish high wettability with a low porosity and a high roughness, resulting in a high self-cleaning number. The possible combinations of printing parameters for optimal self-cleaning ability of all three materials are discussed below.

As Fig. 5 shows, a decrease in the printing speed of 30 mm/min led to porosity due to the high staircase effect. In some circumstances, a flow rate of 50% can be changed to a working value to reduce the staircase effect. Reducing the print temperature to 240^0C significantly decreased the best value. The porosity of the 3D-printed object was less affected by its printing speed. Fig. 9 displays a smoother porosity as D increases in the accompanying graph. Given that the extruded material has more time to spread and generate rough or uneven layers, as shown in Fig. 6, this lower-temperature print could produce a porosity quality.

The plot also makes it evident that printing speed (C), flow rate (B), and print temperature (A) are the three factors that have the most influence on porosity.

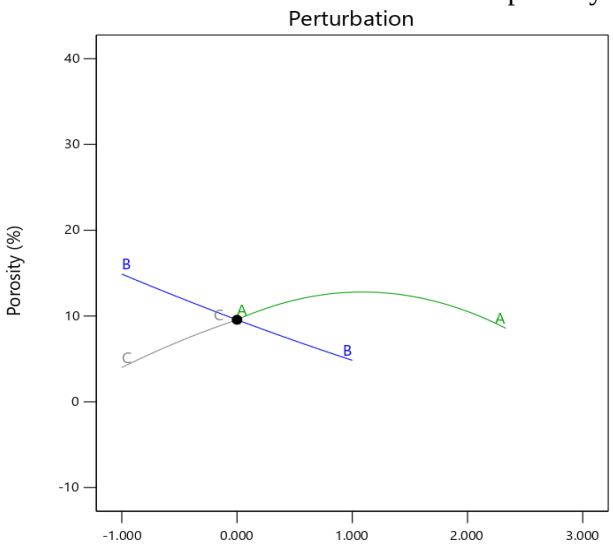

Fig. 6 Perturbation plot illustrating how process parameters 3D-printed textiles affect the fabric's porosity

Figures 7 and 8 show the effect of the interaction of printing temperature with flow rate and printing speed on porosity, respectively. Fig. 9 shows the effect of flow rate and printing speed on porosity. The corresponding 2D and 3D contour plots in Figs. 7(a) and 7(b) show the effect of flow rate and printing temperature on porosity to maintain the self-cleaning property.

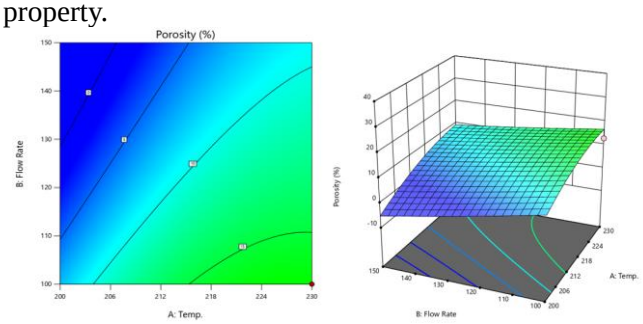

Fig. 7 The contour graphs shown in the (a) 2D and (b) 3D plots illustrate how printing temperature and flow rate affect the porosity of the self-cleaning surface

Figs. 8(a) and 8(b) show the contour plot's center depicted as a concentric circle is where the optimal porosity value. According to the plot, the ideal porosity was at a printing speed of 40 mm/min and a printing temperature of 230°C. The porosity will typically decrease/increase when the printing speed and temperature deviate from the stated parameters obtained at a printing speed of 40 mm/min and a temperature of 230°C. The porosity will typically decrease/increase when the printing speed and temperature deviate from the stated parameters.

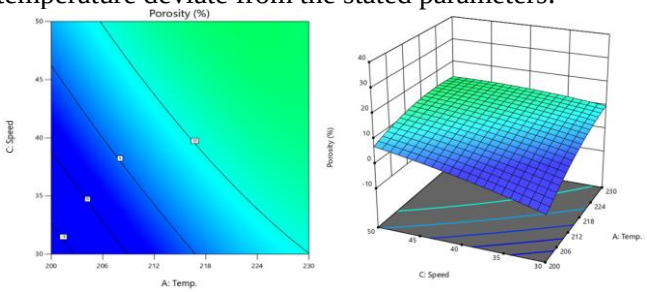

Fig. 8 The contour graphs shown in (a) and (b) illustrate how printing temperature and print speed affect the porosity of the self-cleaning surface

At a constant printing temperature of 230°C, Fig. 9 shows the interaction effect of printing speed and flow rate. As shown in the 2D and 3D contour plots, an ideal porosity of 2.1% is roughly obtained at a printing speed of 40 mm/min and a flow rate of 50%.

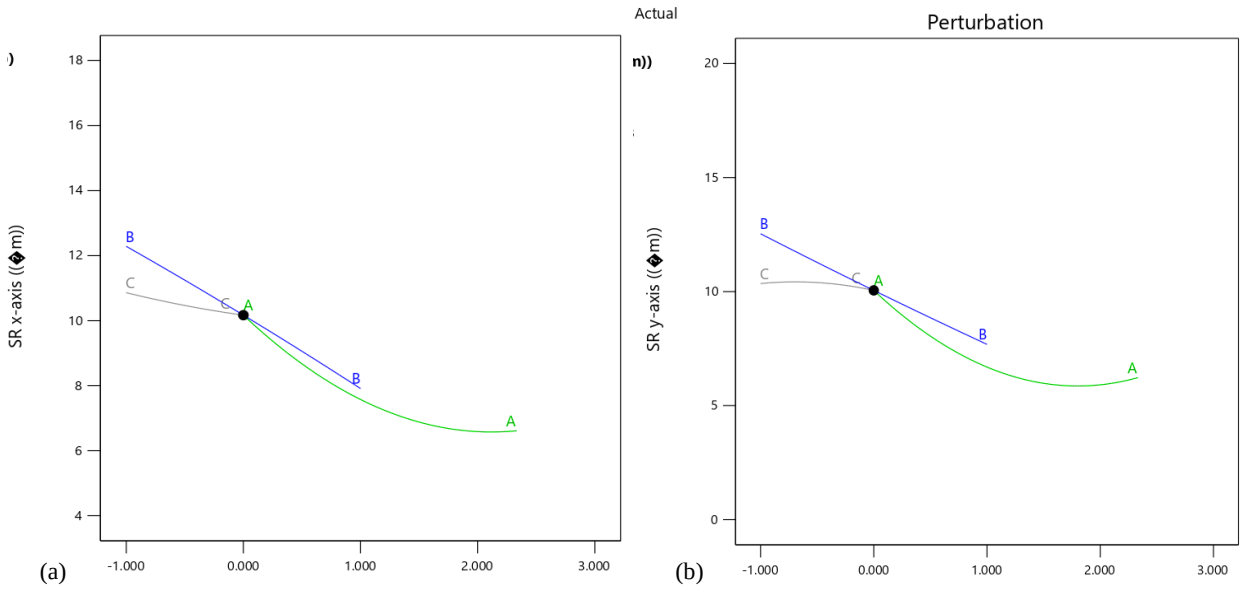

Fig. 9 The contour graphs shown in (a) and (b) illustrate how the flow rate and print speed affect the porosity of the self-cleaning surface

Fig. 10 shows the impact of the process parameters on the self-cleaning property based on the SR-x and SR-y characteristics in the perturbation plot of an optimal design. Figs. 11, 12, and 13 show the effects of printing speed, flow rate, and printing temperature on SR-x, respectively, whereas Figs. 14, 15, and 16 show the effects of printing speed, flow rate, and printing temperature on SR-y, respectively. The impact of printing speed and flow rate on SR-x and SR-y while maintaining a constant printing temperature of 230°C is depicted in Figs. 14(a) and 14(b).

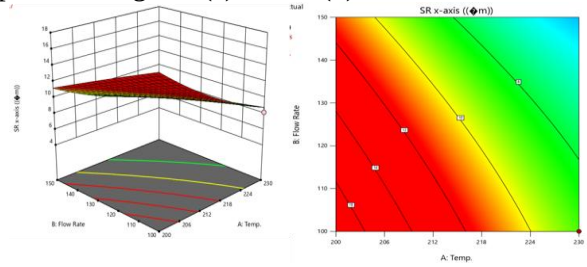

Fig. 10 Perturbation plot that illustrates how process parameters affect the fabric's (a) SR-x and (b) SR-y properties

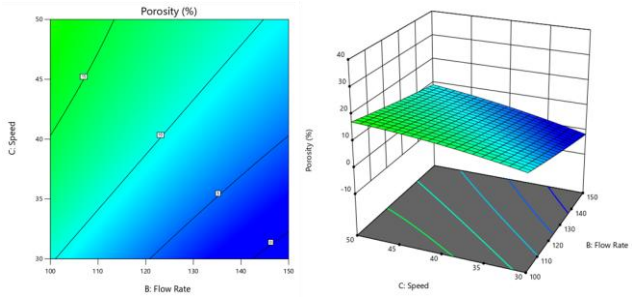

Fig. 11 Contour plots of (a) the 3D contour and (b) the 2D contour showing the impact of printing temperature and flow rate on the SR-x property

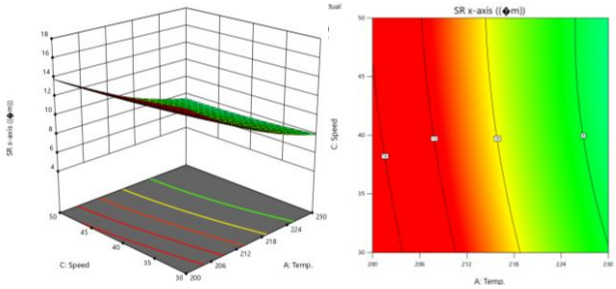

Fig. 12 Contour plots of (a) the 3D contour and (b) the 2D contour showing the impact of printing temperature and flow rate on the SR-y property

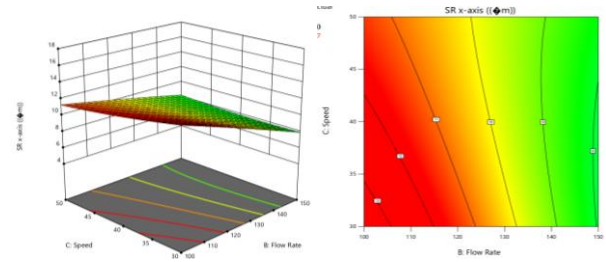

Fig. 12 Contour plots of (a) the 3D contour and (b) the 2D contour showing how printing temperature and print speed affect the SR-x property

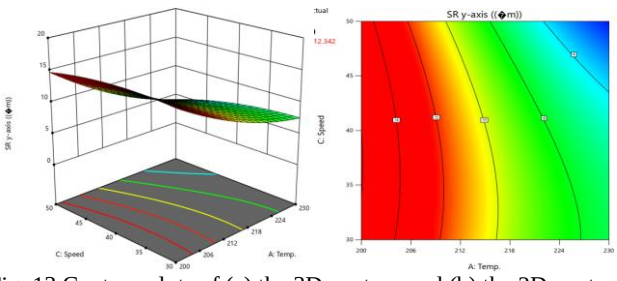

Fig. 13 Contour plots of (a) the 3D contour and (b) the 2D contour showing how printing temperature and print speed affect the SR-y property

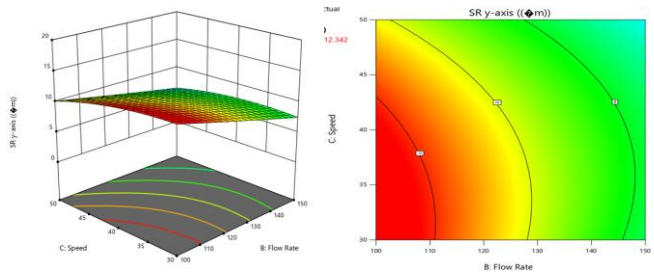

Fig. 14 Contour plots in (a) and (b) showing the effects of flow rate and print speed on the SR-y property

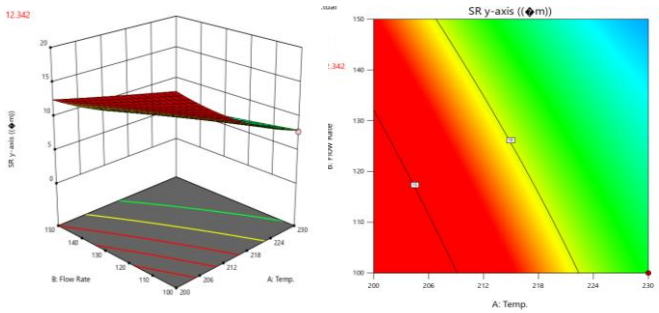

Fig. 15 Contour plots in (a) and (b) showing the effects of flow rate and printing temperature on the SR-y property

3.2. Model Validation

A popular method for multiple response optimization is the desirability function (DF) approach. Harrington in 1965 [26, 28] first introduced the desirability function technique. The ideal operating circumstances (x) for producing the desired response values are identified using this method. All outputs are converted to distinct DFs using a scale factor ranging from 0 to 1. The values for these functions are initialized to the desired, minimal, or maximal output from the experiments.

The optimal process conditions for maximizing the self-cleaning nature of 3D-printed textile parameters are identified by a combination of variables to achieve minimum porosity, SR-x, and SR-y values. Fig. 16 shows the optimized parameters for minimum porosity, SR-x, and SR-y in bar and ramp charts. The optimized parameters obtained include a printing speed of 30 mm/min, a flow rate of 100%, and a printing temperature of 230°C with a desirability value of 0. 549.

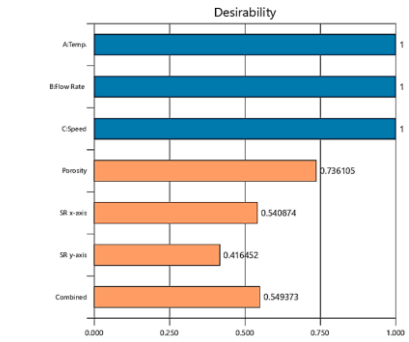

(a)

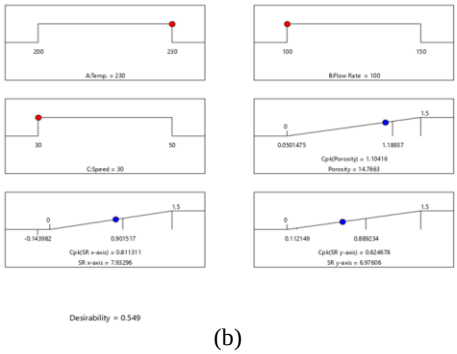

(b)

Fig. 16 Forecasts of ideal process parameters for self-cleaning in (a) bar and (b) ramp graphic

Tables 6 and 7 illustrate the errors computed for all 27 runs used to evaluate the model built using the desirability technique. Table 8 displays the actual value, predicted value, and percentage error for SR-x and SR-y for porosity. Trials determined the actual values and the empirical equations in the design expert software determined the predicted values [27]. As a result, the newly developed models anticipated values for porosity, SR-x, and SR-y are close to the experimental results. Tables 7 and 8 display the results of the validation experiments. The anticipated ideal self-cleaning conditions are also tested in the model. With a printing temperature of 299°C, a flow rate of 150%, and a printing speed of 30 mm/min – Is this Cpk or SR value checked in the criteria?

Table 6 Optimization criteria used in the investigation

Name	Goal	Lower limit	Upper limit	Lower weight	Importance
A: Temp.	is in the range	200	230	1	3
B: Flow rate	is in the range	100	150	1	3
C: Speed	is in the range	30	50	1	3
Porosity	Cpk	2.01	31.43	1	3
SR x-axis	Cpk	4.91	11.7	1	3
SR y-axis	Cpk	4.07699	12.342	1	3

Table 7 Results of the trials along with the predicted values obtained using Point Prediction of the design expert software

Solution	Predicted mean	Predicted median	Std dev	SE mean	95% CI low for mean	95% CI high for mean	95% TI low for 99% pop	95% TI high for 99% pop	Cpk
Porosity	14.7663	14.7663	3.85099	1.96083	10.6293	18.9033	-2.53343	32.066	1.10
SR x-axis	7.93296	7.93296	1.24201	0.632399	6.59872	9.26721	2.35352	13.5124	0.8113
SR y-axis	6.97606	6.97606	1.54697	0.787678	5.31421	8.63792	0.0266421	13.9255	0.6247

Table 8 Results of the trials along with the predicted values obtained using Point Prediction of the design expert software, with comparison for desirability analysis

No.	Temp.	Flow rate	Speed	Porosity	Cpk (Porosity)	SR x-axis	Cpk (SR x-axis)	SR y-axis	Cpk (SR y-axis)	Desirability	
1	230.000	100.000	30.000	14.766	1.104	11.05	0.811	10.6232	0.625	0.549	Selected
2	230.000	100.177	30.000	14.736	1.102	8.26	0.810	8.0007	0.623	0.548	
3	230.000	100.000	30.101	14.742	1.102	5.52	0.810	8.2607	0.623	0.548	
4	229.842	100.000	30.000	14.723	1.100	11.70	0.807	12.3420	0.620	0.546	
5	230.000	100.000	30.245	14.706	1.099	8.27	0.807	8.2607	0.621	0.546	
6	229.982	100.453	30.000	14.684	1.097	5.91	0.807	7.2607	0.621	0.546	
7	230.000	100.000	30.358	14.677	1.096	10.93	0.805	11.2607	0.619	0.545	
8	230.000	100.708	30.000	14.646	1.094	8.19	0.805	7.8170	0.620	0.545	
9	230.000	100.000	30.429	14.659	1.095	4.91	0.804	5.2607	0.618	0.544	
10	229.610	100.002	30.000	14.658	1.095	11.24	0.801	11.2607	0.613	0.542	
11	229.998	101.284	30.000	14.548	1.085	9.10	0.800	8.4395	0.615	0.541	
12	229.334	100.000	30.000	14.579	1.088	5.32	0.793	4.0770	0.605	0.537	
13	230.000	102.010	30.000	14.427	1.075	8.91	0.794	8.8982	0.610	0.536	
14	229.189	100.000	30.000	14.536	1.084	7.92	0.789	7.1795	0.601	0.534	
15	228.971	100.000	30.000	14.470	1.079	5.75	0.783	5.4445	0.595	0.530	
16	230.000	109.383	30.000	13.214	0.970	11.47	0.729	11.2607	0.559	0.489	
17	230.000	109.873	30.000	13.136	0.963	8.91	0.724	8.2607	0.556	0.486	
18	230.000	113.447	30.000	12.569	0.914	5.84	0.691	5.2607	0.532	0.464	
19	230.000	104.999	41.021	9.301	0.631	11.25	0.604	11.2607	0.588	0.405	
20	230.000	123.305	30.000	11.071	0.784	9.29	0.596	9.2607	0.469	0.402	
21	230.000	126.803	30.000	10.561	0.740	6.42	0.561	6.2607	0.448	0.380	
22	230.000	115.279	43.159	6.665	0.403	11.34	0.538	11.2607	0.589	0.336	
23	228.582	129.094	30.000	9.859	0.679	9.56	0.511	9.2607	0.399	0.345	
24	227.868	100.000	30.459	11.615	1.091	6.64	0.400	6.5207	0.313	0.441	
25	226.503	100.000	30.000	11.628	1.092	5.20	0.498	5.2607	0.310	0.440	
26	225.318	100.000	30.000	11.574	1.088	6.54	0.493	6.0820	0.305	0.437	
27	224.998	101.120	30.000	10.521	1.067	7.60	0.300	7.7045	0.343	0.421	

4. Conclusion

The current study carefully examined the effect of process parameter variables such as print temperature, print speed, and flow rate on the porosity and surface roughness of 3D-printed self-cleaning polyurethane using response surface methods in the design and optimization of the experiments and in forecasting the results. The response surface approach determined the linear, interaction, and square effects of the parameters and their influence on the overall dependent property.

1. Porosity and surface roughness are essential characteristics to measure self-cleaning properties [53]. Results obtained from the present study show that the most influential factor affecting the porosity and surface roughness characteristics is the print speed, followed by the flow rate and print temperature. These also show significant relationships between print speed, flow rate, and temperature.

2. The Box–Behnken experimental design established an efficient association between the responses (porosity and surface roughness) and the input parameters (R, T, and S). Tests aimed to optimize the porosity and surface roughness using three different values for each parameter.

3. Using 2D and 3D contour plots and perturbation graphs, the impacts of 3D printing parameter interactions were studied, recording that temperature is the most influential among all. The optimal printing conditions obtained were T=230°C, 30 mm/min print speed, and 100% flow rate.

4. The results were successfully applied to the desirability strategy. The ideal values for porosity, surface roughness-x, and surface roughness-y were 14.766 Ra, 7.933 Ra, and 6.976 Ra, respectively, at a matching flow rate of 100, a print speed of 30 mm/min, and temperature of 230°C.

5. The newly built model was validated for porosity and surface roughness prediction by comparing the results of all 27 trials with the anticipated results for the same experimental work conditions. Surface roughness had a minimum percentage error of -1.550 and a minimum percentage error of -6.133 for porosity. Porosity and surface roughness levels that were very similar to the experimental data accurately predicted by the newly constructed model.

References

[1] QUAN Y.-Y., ZHANG L.-Z., QI R.-H., and CAI R.-R. Self-cleaning of surfaces: the role of surface wettability and dust types. *Scientific Reports*, 2016, 6: 38239. https://doi.org/10.1038/srep38239

[2] ATWAH A.A., and KHAN M.A. Influence of microscopic features on the self-cleaning ability of textile fabrics. *Textile Research Journal*, 2022, 93(1-2). https://doi.org/10.1177/00405175211069881

[3] HASAN M.S., and NOSONOVSKY M. Lotus effect and friction: does nonsticky mean slippery? *Biomimetics*, 2020, 5. https://doi.org/10.3390/biomimetics5020028

[4] VIZITEU D.-R., and CURTEZA A. 3D printing technology in textile and fashion industry. *Fashion Industry*, 2021, 3: 41-44. https://doi.org/10.30857/2706-5898.2020.3.2

[5] XIAO Y.Q., and KAN C.W. Review on development and application of 3D-printing technology in textile and fashion design. *Coatings*, 2022, 12.

https://doi.org/10.3390/coatings12020267

[6] KORGER M., BERGSCHNEIDER J., LUTZ M., MAHLTIG B., FINSTERBUSCH K., and RABE M. Possible applications of 3D printing technology on textile substrates. *IOP Conference Series: Materials Science and Engineering*, 2016, 141: 012011. https://doi.org/10.1088/1757-899X/141/1/012011

[7] DIP T.M., EMU A.S., NAFIZ M.N.H., KUNDU P., RAKHI H.R., SAYAM A., AKHTARUJJMAN M., SHOAIB M., AHMED M.S., USHNO S.T., ASHEQUE A.I., HASNAT E., UDDIN M.A., and SAYEM A.S.M. 3D printing technology for textiles and fashion. *Textile Progress*, 2020, 52. https://doi.org/10.1080/00405167.2021.1978223

[8] PARTSCH L., VASSILIADIS S., and PAPAGEORGAS P. 3D printed textile fabrics structures. In: *5th International Istanbul Textile Congress 2015: Innovative Technologies "Inspire to Innovate."* 2015.

[9] FORMAN J., DOGAN M.D., FORSYTHE H., and ISHII H. DefeXtiles: 3D printing quasi-woven fabric via under-extrusion. In: *UIST 2020 – Proceedings of the 33rd Annual ACM Symposium on User Interface Software and Technology*, 2020, https://doi.org/10.1145/3379337.3415876

[10] TAKAHASHI H., and KIM J. 3D printed fabric: techniques for design and 3D weaving programmable textiles. In: *UIST 2019 – Proceedings of the 32nd Annual ACM Symposium on User Interface Software and Technology*. 2019. https://doi.org/ 10.1145/3332165.3347896

[11] PATTINSON S.W., HUBER M.E., KIM S., LEE J., GRUNSFELD S., ROBERTS R., DREIFUS G., MEIER C., LIU L., HOGAN N., and HART A.J. Additive manufacturing of biomechanically tailored meshes for compliant wearable and implantable devices. *Advanced Functional Materials*, 2019, 29. https://doi.org/10.1002/adfm.201901815

[12] XIAO Y.Q., and KAN C.W. Review on development and application of 3D-printing technology in textile and fashion design. *Coatings*, 2022, 12. https://doi.org/ 10.3390/coatings12020267

[13] HE F., THAKUR V.K., and KHAN M. Evolution and new horizons in modeling crack mechanics of 3D printing polymeric structures. *Materials Today Chemistry*, 2021, 20: 100393. https://doi.org/10.1016/j.mtchem.2020.100393

[14] POORNAGANTI S., YEOLE S.N., and KODE J.P. Insights on surface characterization of 3D printed polymeric parts. *Materials Today: Proceedings*, 2022, 62: 3837-3848. https://doi.org/10.1016/J.MATPR.2022.04.499

[15] LEE K.-M., PARK H., KIM J., and CHUN D.-M. Fabrication of a superhydrophobic surface using a fused deposition modeling (FDM) 3D printer with poly lactic acid (PLA) filament and dip coating with silica nanoparticles. *Applied Surface Science*, 2019, 467-468: 979-991. https://doi.org/10.1016/j.apsusc.2018.10.205

[16] KIM M.K., LEE I.H., and KIM H.C. Effect of fabrication parameters on surface roughness of FDM parts. *International Journal of Precision Engineering and Manufacturing*, 2018, 19: 137-142. https://doi.org/10.1007/S12541-018-0016-0

[17] SRINIVASAN R., RUBAN W., DEEPANRAJ A., BHUVANESH R., and BHUVANESH T. Effect on infill density on mechanical properties of PETG part fabricated by fused deposition modelling. *Materials Today: Proceedings*, 2020, 27: 1838-1842. https://doi.org/10.1016/J.MATPR.2020.03.797

[18] BUJ-CORRAL I., BAGHERI A., and SIVATTE-ADROER M. Effect of printing parameters on dimensional error, surface roughness and porosity of FFF printed parts with grid structure. *Polymers*, 2021, 13. https://doi.org/10.3390/polym13081213

[19] TURA A.D., MAMO H.B., and GEMECHU W.F. Mathematical modeling and parametric optimization of surface roughness for evaluating the effects of fused deposition modeling process parameters on ABS material. *International Journal of Advanced Engineering Research and Science*, 2021, 8(5).

[20] BARRIOS J.M., and ROMERO P.E. Improvement of Surface Roughness and Hydrophobicity in PETG Parts Manufactured via Fused Deposition Modeling (FDM): An Application in 3D Printed Self-Cleaning Parts. *Materials*, 2019, 12: 2499. https://doi.org/10.3390/ma12152499

[21] SRINIVASAN R., RUBAN W., DEEPANRAJ A., BHUVANESH R., and BHUVANESH T. Effect on infill density on mechanical properties of PETG part fabricated by fused deposition modelling. *Materials Today: Proceedings*, 2020, 27(2): 1838-1842. https://doi.org/10.1016/j.matpr.2020.03.797

[22] PEI X., ZHANG S., ZHANG W., ADNAN ATWAH A., DUKHI ALMUTAIRI M., HE, F. and KHAN M.A. Influence of Printing Parameters on Self-Cleaning Properties of 3D Printed Polymeric Fabrics. *Polymers*, 2022, 14(15): 3128. https://doi.org/10.3390/polym14153128

[23] KHURI A.I., and MUKHOPADHYAY S. Response surface method. *Willey Interdiciplinary Reviews*, 2010, 2(2): 128-149. https://doi.org/10.1002/wics.73

[24] PALANI P., and MURUGAN N. Optimization of weld bead geometry for stainless steel claddings deposited by FCAW. *Journal of Materials Processing Technology*, 2007, 190(1-3): 291-299. http://dx.doi.org/10.1016/j.jmatprotec.2007.02.035

[25] SABRY I.M., IDRISI A.N., and MOURAD A.-H.I. Friction stir welding process parameters optimization through hybrid multi-criteria decision-making approach. *International Review on Modelling and Simulations*, 2021, 14(1): 32-43. http://dx.doi.org/10.15866/iremos.v14i1.19537

[26] SABRY I., MOURAD A.-H.I., and THEKKUDEN D.T. Optimization of metal inert gas welded aluminium 6061 pipe parameters using analysis of variance and grey relational analysis. *SN Applied Sciences*, 2020, 2(3): 175-185. https://link.springer.com/article/10.1007/s42452-020-1943-9

[27] SABRY I., GADALLAH N., and ABU-OKAIL M. Optimization of friction stir welding parameters using response surface methodology. *IOP Conference Series: Materials Science and Engineering*, 2020, 973: 012017. DOI: 10.1088/1757-899X/973/1/012017

[28] EL-ATTAR T., SABRY I., and EL-ASSAL A. Multi-objective Optimization on Surface Roughness of 3D-Printed Parts by Fused Deposition Modelling. In: *2022 4th Novel Intelligent and Leading Emerging Sciences Conference (NILES)*, 2022: 331-334. DOI: 10.1109/NILES56402.2022.9942401

[29] AHMED F.M., REDA M.M., EL-AZIZ H.A.A., and OTHMAN H.A. Overview of Different Fabric Structures. *Journal of Textiles, Coloration and Polymer Science*, 2022, 19(2): 291-306.

[30] AHMED F.M., REDA M.M., EL-AZIZ H.A.A., and OTHMAN H.A. Innovative Designs for One-Piece Clothing

Inspired by the Textures and Color of Macrame and Carpet Stitches. *Journal of Textiles, Coloration and Polymer Science*, 2022, 19(2): 245-267.
[31] XIE L., CHEN X., WEN Z., YANG Y., SHI J., CHEN C., PENG M., LIU Y., and SUN X. Spiral steel wire based fiber-shaped stretchable and tailorable triboelectric nanogenerator for wearable power source and active gesture sensor. *Nano-Micro Letters*, 2019, 11, Article number: 39.
[32] DONG K., PENG X., AN J., WANG A.C., LUO J., SUN B., WANG J., and WANG Z.L. Shape adaptable and highly resilient 3D braided triboelectric nanogenerators as e-textiles for power and sensing. *Nature Communications*, 2020, 11: 2868.
[33] ZHAO Z., HUANG Q., YAN C., LIU Y., ZENG X., WEI X., HU Y., and ZHENG Z. Machinewashable and breathable pressure sensors based on triboelectric nanogenerators enabled by textile technologies. *Nano Energy*, 2020, 70: 104528.
[34] DAI Y., FU Y., ZENG H., XING L., ZHANG Y., ZHAN Y., and XUE X. A self-powered brainlinked vision electronic-skin based on triboelectric-photodetecing pixeladdressable matrix for visual-image recognition and behavior intervention. *Advanced Functional Materials*, 2018, 28: 1800275.
[35] WANG L., and DAOUD W.A. Highly flexible and transparent polyionic-skin triboelectric nanogenerator for biomechanical motion harvesting, advanced energy. *Materials*, 2019, 9: 1803183.
[36] WANG W., YU A., LIU X., LIU Y., ZHANG Y., ZHU Y., LEI Y., JIA M., ZHAI J., and WANG Z.L. Large-scale fabrication of robust textile triboelectric nanogenerators. *Nano Energy*, 2020, 71: 104605.
[37] PENG X., DONG K., YE C., JIANG Y., ZHAI S., CHENG R., LIU D., GAO X., WANG J., and WANG Z.L. A breathable, biodegradable, antibacterial, and self-powered electronic skin based on all-nanofiber triboelectric nanogenerators. *Science Advances*, 2020, 6: 9624.
[38] XIE L., CHEN X., WEN Z., YANG Y., SHI J., CHEN C., PENG M., LIU Y., and SUN X. Spiral steel wire based fiber-shaped stretchable and tailorable triboelectric nanogenerator for wearable power source and active gesture sensor. *Nano-Micro Letters*, 2019, 11, Article number: 39.
[39] DONG K., PENG X., AN J., WANG A.C., LUO J., SUN B., WANG J., and WANG Z.L. Shape adaptable and highly resilient 3D braided triboelectric nanogenerators as e-textiles for power and sensing. *Nature Communications*, 2020, 11: 2868.
[40] ZHAO Z., HUANG Q., YAN C., LIU Y., ZENG X., WEI X., HU Y., and ZHENG Z. Machinewashable and breathable pressure sensors based on triboelectric nanogenerators enabled by textile technologies. *Nano Energy*, 2020, 70: 104528.
[41] PAOSANGTHONG W., WAGIH M., TORAH R., and BEEBY S. Textile-based triboelectric nanogenerator with alternating positive and negative freestanding grating structure. *Nano Energy*, 2019, 66: 104148.
[42] KUMAR D., WU X., FU Q., HO J.W.C., KANHERE P.D., LI L., and CHEN Z. Hydrophobic sol-gel coatings based on polydimethylsiloxane for self-cleaning applications. *Materials and Design*, 2015, 86: 855-862.
[43] KUMAR D., WU X., FU Q., HO J.W.C., KANHERE P.D., LI L., and CHEN Z. Development of durable self-cleaning coatings using organic-inorganic hybrid sol-gel method. *Applied Surface Science*, 2015, 344: 205-212.
[44] FU Q., WU X., KUMAR D., HO J.W.C., KANHERE P.D., SRIKANTH N., LIU E., WILSON P., and CHEN Z. Development of sol−gel icephobic coatings: effect of surface roughness and surface energy. *ACS Applied Materials and Interfaces*, 2014, 6(23): 20685-20692. https://doi.org/10.1021/am504348x
[45] KARMOUCH R., and ROSS G.G. Superhydrophobic wind turbine blade surfaces obtained by a simple deposition of silica nanoparticles embedded in epoxy. *Applied Surface Science*, 2010, 257(3): 665-669.
[46] BARKHUDAROV P.M., SHAH P.B, WATKINS E.B., DOSHI D.A., BRINKER C.J., and MAJEWSKI J. Corrosion inhibition using superhydrophobic films. *Corrosion Science*, 2008, 50: 897-902.
[47] CHEN R., ZHANG X., SU Z., GONG R., GE X., ZHANG H., and WANG C. Perfectly hydrophobic silicone nanofiber coatings: preparation from Methyltrialkoxysilanes and use as water-collecting substrate. *Journal of Physical Chemistry C*, 2009, 113: 8350-8356.
[48] ZHAI L., CEBECI F.C., COHEN R.E., and RUBNER M.F. Stable superhydrophobic coatings from polyelectrolyte multilayers. *Nano Letters*, 2004, 4: 1349-1353.
[49] BALU B., BREEDVELD V., and HESS D.W. Fabrication of "roll-off" and "sticky" superhydrophobic cellulose surfaces via plasma processing. *Langmuir*, 2008, 24(9): 4785-4790.
[50] AL-QADHI M., MERAH N., MATIN A., ABU-DHEIR N., KHALED M., and YOUCEF-TOUMI K. Preparation of superhydrophobic and self-cleaning polysulfone non-wovens by electrospinning: influence of process parameters on morphology and hydrophobicity. *Journal of Polymer Research*, 2015, 22: 207.
[51] LIU X., and HE J. One-step hydrothermal creation of hierarchical microstructures toward superhydrophilic and superhydrophobic surfaces. *Langmuir*, 2009, 25: 11822-11826.
[52] MCHALE G., AQIL S., SHIRTCLIFFE N.J., NEWTON M.I., and ERBIL H.Y. Analysis of droplet evaporation on a superhydrophobic surface. *Langmuir*, 2005, 21: 11053-11060.
[53] ATWAH A.A., ALMUTAIRI M.D., HE F., and KHAN M.A. Influence of Printing Parameters on Self-Cleaning Properties of 3D Printed Polymeric Fabrics. *Polymers*, 2022, 14: 3128. https://doi.org/10.3390/polym14153128
[54] BABU S.S., MOURAD A.H.I., HARIB K.H., and VIJAYAVENKATARAMAN S. Recent developments in the application of machine-learning towards accelerated predictive multiscale design and additive manufacturing. *Virtual and Physical Prototyping*, 2023, 18(1): 2141653.
[55] BABU S.S., MOURAD A.H.I., and HARIB K.H. Unauthorized usage and cybersecurity risks in additively manufactured composites: Toolpath reconstruction using imaging and machine learning techniques. In: *2022 Advances in Science and Engineering Technology International Conferences (ASET)*, 2022: 1-7. http://dx.doi.org/10.1109/ASET53988.2022.9734313
[56] BABU S.S., and MOURAD A.H.I. Multiscale Modelling of Multifunctional Composites: A Review. In: *ASME International Mechanical Engineering Congress and Exposition.* 2021. http://dx.doi.org/10.1115/IMECE2021-73276
[57] AL JASSMI H., AL NAJJAR F., and MOURAD A.H.I. Large-Scale 3D printing: The way forward. *IOP Conference*

Series: Materials Science and Engineering, 2018, 324: 012088.
[58] RAHMANI A., and MOURAD A.H.I. On the use of additive manufacturing for mechanical performance assessment of engineering materials: a review. In: *2020 Advances in Science and Engineering Technology International Conferences (ASET)*, 2020: 1-5.
[59] MOURAD A.H.I. Special collection on recent trends in design and additive manufacturing. *Advances in Mechanical Engineering*, 2019, 11(12). http://dx.doi.org/10.1177/1687814019890695
[60] MOURAD A.I., GHAZAL A.M., SYAM M.M., AL QADI O.D., and AL JASSMI H. Utilization of Additive Manufacturing in Evaluating the Performance of Internally Defected Materials. *IOP Conference Series: Materials Science and Engineering*, 2018, 362(1): 012026.

参考文:

[1] QUAN Y.-Y., ZHANG L.-Z., QI R.-H. 和 CAI R.-R. 表面自清潔：表面潤濕性和灰塵類型的作用。科學報告，2016 年，6：38239。https://doi.org/10.1038/srep38239
[2] ATWAH A.A. 和 KHAN M.A. 微觀特徵對紡織布料自清潔能力的影響。紡織研究雜誌，2022，93（1-2）。https://doi. 組織/10.1177/00405175211069881
[3] HASAN M.S. 和 NOSONOVSKY M. 蓮花效應和摩擦力：不黏就意味著滑嗎？仿生學，2020，5。https://doi.org/10.3390/biomimetics5020028
[4] VIZITEU D.-R. 和 CURTEZA A. 紡織和時尚產業的三維列印技術。時尚產業，2021，3：41-44。https://doi.org/10.30857/2706-5898.2020.3.2
[5] XIAO Y.Q. 和 KAN C.W. 三維列印技術在紡織服裝設計中的發展與應用綜述。塗料，2022 年，12。https://doi.org/10.3390/coatings12020267
[6] KORGER M.、BERGSCHNEIDER J.、LUTZ M.、MAHLTIG B.、FINSTERBUSCH K. 和 RABE M. 三維列印技術在紡織基材上的可能應用。物理研究所會議系列：材料科學與工程，2016，141：012011。https://doi.org/10.1088/1757-899X/141/1/012011
[7] DIP T.M., EMU A.S., NAFIZ M.N.H., KUNDU P., RAKHI H.R., SAYAM A., AKHTARUJJMAN M., SHOAIB M., AHMED M.S., USHNO S.T., ASHEQUE A.I., HASNAT E., UDDIN M.A. 和 SAYEM A.S.M. 用於紡織品和時裝的 三維 列印技術。紡織進展，2020 年，52。https://doi.org/10.1080/00405167.2021.1978223
[8] PARTSCH L.、VASSILIADIS S. 和 PAPAGEORGAS P. 三維 列印紡織布料結構。參見：2015 年第五屆伊斯坦堡國際紡織大會：創新技術「激發創新」。2015 年。
[9] FORMAN J.、DOGAN M.D.、FORSYTHE H. 和 ISHII H. 德菲克斯泰尔斯：透過欠擠壓 三維 列印準編織物。請參閱：使用者介面軟體和技術 2020–第 33 屆計算機協會使用者介面軟體與技術年度研討會論文集，2020 年，https://doi.org/10.1145/3379337.3415876
[10] TAKAHASHI H. 和 KIM J. 三維 列印織物：設計和三維 編織可程式紡織品的技術。請參閱：使用者介面軟體和技術 2019–第 32 屆計算機協會使用者介面軟體與技術年度研討會論文集。2019。https://doi.org/10.1145/3332165.3347896
[11] PATTINSON S.W.、HUBER M.E.、KIM S.、LEE J.、GRUNSFELD S.、ROBERTS R.、DREIFUS G.、MEIER C.、LIU L.、HOGAN N. 與 HART A.J. 用於合規可穿戴和可植入設備的生物力學客製化網格的積層製造。先進功能材料，2019，29。https://doi.org/10.1002/adfm.201901815
[12] XIAO Y.Q. 和 KAN C.W. 三維列印技術在紡織服裝設計中的發展與應用綜述。塗料，2022 年，12。https://doi.org/10.3390/coatings12020267
[13] HE F.、THAKUR V.K. 和 KHAN M. 三維 列印聚合物結構裂紋力學建模的演變和新視野。今日材料化學，2021，20：100393。https://doi.org/10.1016/j.mtchem.2020.100393
[14] POORNAGANTI S.、YEOLE S.N. 和 KODE J.P. 關於 三維 列印聚合物零件表面特性的見解。今日材料：會議記錄，2022 年，62：3837-3848。https://doi.org/10.1016/J.MATPR.2022.04.499
[15] LEE K.-M.，PARK H.，KIM J. 和 CHUN D.-M.。使用熔融沈積成型三維 列印機、聚乳酸絲和浸塗二氧化矽奈米粒子來製造超疏水錶面。應用表面科學，2019，467-468：979-991。https://doi.org/10.1016/j.apsusc.2018.10.205
[16] KIM M.K.、LEE I.H. 和 KIM H.C. 製造參數對熔融沈積建模零件表面粗糙度的影響。國際精密工程與製造雜誌，2018，19：137-142。https://doi.org/10.1007/S12541-018-0016-0
[17] SRINIVASAN R.、RUBAN W.、DEEPANRAJ A.、BHUVANESH R. 和 BHUVANESH T. 填充密度對熔融沈積建模製造的聚對苯二甲酸乙二酯零件機械性能的影響。今日材料：會議記錄，2020 年，27：1838-1842。https://doi.org/10.1016/J。MATPR.2020.03.797
[18] BUJ-CORRAL I.、BAGHERI A. 和 SIVATTE-ADROER M. 列印參數對網格結構 FFF 列印零件尺寸誤差、表面粗糙度和孔隙率的影響。聚合物，2021 年，13。https://doi.org/10.3390/polym13081213
[19] TURA A.D.、MAMO H.B. 和 GEMECHU W.F. 表面粗糙度的數學建模和參數最佳化，用於評估熔融沈積建模製程參數對丙烯腈-丁二烯-苯乙烯材料的影響。國際先進工程研究與科學雜誌，2021，8（5）。
[20] BARRIOS J.M. 和 ROMERO P.E. 透過熔融沈積成型改善聚對苯二甲酸乙二酯零件的表面粗糙度和疏水性：在 三維 列印自清潔零件中的應用。資料，2019，12：2499。https://doi.org/10.3390/ma12152499
[21] SRINIVASAN R.、RUBAN W.、DEEPANRAJ A.、BHUVANESH R. 和 BHUVANESH T. 填充密度對熔融沈積建模製造的聚對苯二甲酸乙二酯零件機械性能的影響。今日材料：會議記錄，2020 年，27(2)：1838-1842。https://doi.org/10.1016/j.matpr.2020.03.797
[22] PEI X., ZHANG S., ZHANG W., ADNAN ATWAH A., DUKHI ALMUTAIRI M., HE, F. 和 KHAN M.A. 列印參數對 三維 列印聚合物織物自清潔性能的影響。聚合物，2022, 14(15): 3128. https://doi.org/10.3390/polym14153128
[23] KHURI A.I.，和 MUKHOPADHYAY S. 響應面法。威利跨學科評論，2010，2(2)：128-149。https://doi.org/10.1002/wics.73
[24] PALANI P. 和 MURUGAN N. 电弧焊沉積不銹鋼覆層焊道幾何形狀的最佳化。材料加工技術, 2007, 190(1-3): 291-299。

http://dx.doi.org/10.1016/j.jmatprotec.2007.02.035
[25] SABRY I.M.、IDRISI A.N. 和 MOURAD A.-H.I. 透過混合多準則決策方法優化攪拌摩擦焊製程參數。國際建模與模擬評論，2021，14(1)：32-43。http://dx.doi.org/10.15866/iremos.v14i1.19537
[26] SABRY I.、MOURAD A.-H.I. 和 THEKKUDEN D.T. 使用變異數分析和灰色關聯分析優化金屬惰性氣體焊接鋁 6061 管路參數。序列号應用科學，2020，2(3)：175-185。 https://link.springer.com/article/10.1007/s42452-020-1943-9
[27] SABRY I.、GADALLAH N. 和 ABU-OKAIL M。使用響應面法優化攪拌摩擦焊接參數。物理研究所會議系列：材料科學與工程，2020，973：012017。DOI：10.1088/1757-899X/973/1/012017
[28] EL-ATTAR T.、SABRY I. 和 EL-ASSAL A。透過熔融沈積建模對三維 列印零件表面粗糙度進行多目標最佳化。請參閱：2022 年第四屆新型智慧與領先新興科學會議，2022：331-334。DOI：10.1109/NILES56402.2022.9942401
[29] AHMED F.M.、REDA M.M.、EL-AZIZ H.A.A. 和 OTHMAN H.A. 不同織物結構的概述。紡織染色與高分子科學期刊, 2022, 19(2): 291-306.
[30] AHMED F.M.、REDA M.M.、EL-AZIZ H.A.A. 和 OTHMAN H.A. 一件式服裝的創新設計，靈感來自蕾絲和地毯縫線的紋理和顏色。紡織、染色與高分子科學學報, 2022, 19(2): 245-267.
[31] XIE L., CHEN X., WEN Z., YANG Y., SHI J., CHEN C., PENG M., LIU Y. 和 SUN X. 螺旋鋼絲基纖維狀可拉伸可剪裁摩擦電用於可穿戴電源和主動手勢感測器的奈米發電機。奈米微快報，2019，11，文章編號：39。
[32] DONG K., PENG X., AN J., WANG A.C., LUO J., SUN B., WANG J. 和 WANG Z.L. 形狀適應性強且高彈性的 三維編織摩擦奈米發電機作為用於電力和感測的電子紡織品。自然通訊，2020，11：2868。
[33] ZHAO Z., HUANG Q., YAN C., LIU Y., ZENG X., WEI X., HU Y. 和 ZHENG Z. 基於紡織技術的摩擦奈米發電機的可機洗和透氣壓力感應器. 奈米能源，2020，70：104528。
[34] DAI Y., FU Y., ZENG H., XING L., ZHANG Y., ZHAN Y. 和 XUE X. 基於摩擦電光電檢測像素可尋址矩陣的自供電腦聯視覺電子皮膚圖像識別和行為介入。先進功能材料，2018，28：1800275。
[35] WANG L. 和 DAOUD W.A. 用於生物力學運動採集的高度靈活和透明的聚離子皮膚摩擦電奈米發電機，先進的能量。材料，2019，9：1803183。
[36] WANG W., YU A., LIU X., LIU Y., ZHANG Y., ZHU Y., LEI Y., JIA M., ZHAI J. 和 WANG Z.L. 大規模製造堅固的紡織摩擦奈米發電機。奈米能源，2020，71：104605。
[37] PENG X., DONG K., YE C., JIANG Y., ZHAI S., CHENG R., LIU D., GAO X., WANG J. 和 WANG Z.L. 基於全奈米纖維摩擦奈米發電機的透氣、可生物降解、抗菌、自供電電子皮膚。科學進展，2020，6：9624。
[38] XIE L., CHEN X., WEN Z., YANG Y., SHI J., CHEN C., PENG M., LIU Y. 和 SUN X. 螺旋鋼絲基纖維狀可拉伸可剪裁摩擦電用於可穿戴電源和主動手勢感測器的奈米發電機。奈米微快報，2019，11，文章編號：39。
[39] DONG K., PENG X., AN J., WANG A.C., LUO J., SUN B., WANG J. 和 WANG Z.L. 形狀適應性強且高彈性的 三維編織摩擦奈米發電機作為用於電力和感測的電子紡織品。自然通訊，2020，11：2868。
[40] ZHAO Z., HUANG Q., YAN C., LIU Y., ZENG X., WEI X., HU Y. 和 ZHENG Z. 基於紡織技術的摩擦奈米發電機的可機洗和透氣壓力感應器. 奈米能源，2020，70：104528。
[41] PAOSANGTHONG W.、WAGIH M.、TORAH R. 和 BEEBY S. 具有交替正負獨立式光柵結構的基於紡織品的摩擦奈米發電機。奈米能源，2019，66：104148。
[42] KUMAR D.、WU X.、FU Q.、HO J.W.C.、KANHERE P.D.、LI L. 和 CHEN Z. 用於自清潔應用的基於聚二甲基矽氧烷的疏水性溶膠-凝膠塗層。材料與設計，2015，86：855-862。
[43] KUMAR D.，WU X.，FU Q.，HO J.W.C.，KANHERE P.D.，LI L. 和 CHEN Z. 使用有機-無機混合溶膠-凝膠方法開發耐用自清潔塗層。應用表面科學，2015，344：205-212。
[44] FU Q., WU X., KUMAR D., HO J.W.C., KANHERE P.D., SRIKANTH N., LIU E., WILSON P. 和 CHEN Z. 溶膠凝膠疏冰塗層的開發：表面粗糙度和表面能。美國化學會應用材料與介面，2014，6(23)：20685-20692。https://doi.org/10.1021/am504348x
[45] KARMOUCH R. 和 ROSS G.G. 透過簡單沉積嵌入環氧樹脂中的二氧化矽奈米粒子獲得超疏水風力渦輪機葉片表面。應用表面科學, 2010, 257(3): 665-669。
[46] BARKHUDAROV P.M., SHAH P.B、WATKINS E.B.、DOSHI D.A.、BRINKER C.J. 和 MAJEWSKI J. 使用超疏水膜抑制腐蝕。腐蝕科學，2008，50：897-902。
[47] CHEN R., ZHANG X., SU Z., GONG R., GE X., ZHANG H. 和 WANG C. 完全疏水性有機矽奈米纖維塗層：甲基三烷氧基矽烷的製備及其作為集水基底的應用。物理化學期刊 C, 2009, 113: 8350-8356。
[48] ZHAI L.、CEBECI F.C.、COHEN R.E. 和 RUBNER M.F. 由聚電解質多層形成的穩定超疏水塗層。奈米快報，2004 年，4：1349-1353。
[49] BALU B.、BREEDVELD V. 和 HESS D.W. 透過等離子體處理製造「滾落」和「黏性」超疏水纖維素表面。朗繆爾，2008，24(9)：4785-4790。
[50] AL-QADHI M.、MERAH N.、MATIN A.、ABU-DHEIR N.、KHALED M. 和 YOUCEF-TOUMI K. 透過靜電紡絲製備超疏水和自清潔聚砜非織造布：製程的影響形態和疏水性參數。高分子研究雜誌，2015，22：207。
[51] LIU X. 和 HE J.一步水熱創造超親水和超疏水錶面的分級微結構。朗繆爾，2009，25：11822-11826。
[52] MCHALE G.、AQIL S.、SHIRTCLIFFE N.J.、NEWTON M.I. 和 ERBIL H.Y. 超疏水錶面上液滴蒸發的分析。朗繆爾，2005 年，21：11053-11060。
[53] ATWAH A.A.、ALMUTAIRI M.D.、HE F. 和 KHAN M.A. 列印參數對 三維列印聚合物織物自清潔性能的影響。聚合物，2022，14：3128。https://doi.org/10.3390/polym14153128
[54] BABU S.S.、MOURAD A.H.I.、HARIB K.H. 和 VIJAYAVENKATARAMAN S. 機器學習在加速預測多尺度設計和增材製造方面的應用的最新進展。虛擬與實體原型，2023, 18(1): 2141653。
[55] BABU S.S.、MOURAD A.H.I. 和 HARIB K.H. 積層

製造複合材料中的未經授權使用和網路安全風險：使用成像和機器學習技術重建刀具路徑。請參閱：2022 年科學與工程技術國際會議進度，2022 年：1-7。http://dx.doi.org/10.1109/ASET53988.2022.9734313
[56] BABU S.S.和 MOURAD A.H.I. 多功能複合材料的多尺度建模：回顧。請參閱：美國機械工程師學會國際機械工程大會暨博覽會。2021. http://dx.doi.org/10.1115/IMECE2021-73276
[57] AL JASSMI H.、AL NAJAR F. 和 MOURAD A.H.I. 大規模 三維 列印：前進之路。物理研究所會議系列：材料科學與工程，2018，324：012088。
[58] RAHMANI A. 和 MOURAD A.H.I. 關於使用積層製造進行工程材料機械性質評估：綜述。請參閱：2020 年科學與工程技術國際會議進度，2020：1-5。
[59] 穆拉德·阿希 關於設計和增材製造最新趨勢的特別收藏。機械工程進展，2019，11(12)。http://dx.doi.org/10.1177/1687814019890695
[60] MOURAD A.I.、GHAZAL A.M.、SYAM M.M.、AL QADI O.D. 和 AL JASSMI H. 利用積層製造評估內部瑕疵材料的性能。物理研究所會議系列：材料科學與工程，2018，362(1)：012026。